nanomaterials

MDPI

Article

Trace Amounts of Co_3O_4 Nano-Particles Modified TiO_2 Nanorod Arrays for Boosted Photoelectrocatalytic Removal of Organic Pollutants in Water

Yongling Du [1,*,†], Zhixiang Zheng [2,*,†], Wenzhuo Chang [3], Chunyan Liu [1], Zhiyong Bai [1], Xinyin Zhao [2] and Chunming Wang [1]

[1] College of Chemistry and Chemical Engineering, Lanzhou University, Lanzhou 730000, China; liuchy19@lzu.edu.cn (C.L.); baizhy17@lzu.edu.cn (Z.B.); Wangcm@lzu.edu.cn (C.W.)
[2] Key Laboratory of Evidence Science Techniques Research and Application, Gansu University of Political Science and Law, Lanzhou 730070, China; zhaoxy18409492375@163.com
[3] College of Chemistry and Chemical Engineering, Northwest Normal University, Lanzhou 730000, China; 15800951150@163.com
* Correspondence: dqzhenghao@163.com (Z.Z.); duyl@lzu.edu.cn (Y.D.); Tel.: +86-9318911895 (Y.D.)
† These authors contributed equally to this work.

Abstract: Trace amounts of Co_3O_4 modified TiO_2 nanorod arrays were successfully fabricated through the photochemical deposition method without adding any nocuous reagents. The Co_3O_4/TiO_2 nanorod arrays fabricated in acid solution had the highest photo-electrochemical activity. We elaborated on the mechanism of Co_3O_4-TiO_2 fabricated in different pH value solutions. The Co_3O_4-TiO_2 had a more remarkable photo-electrochemical performance than the pure TiO_2 nanorod arrays owing to the heterojunction between Co_3O_4 and TiO_2. The degradation of methylene blue and hydroquinone was selected as the model reactions to evaluate the photo-electrochemical performance of Co_3O_4-TiO_2 nanorod arrays. The Co_3O_4/TiO_2 nanorod arrays had great potential in waste water treatment.

Keywords: photocatalytic degradation; photo-electrocatalysis; Co_3O_4-TiO_2; dyes; organic pollutants

Citation: Du, Y.; Zheng, Z.; Chang, W.; Liu, C.; Bai, Z.; Zhao, X.; Wang, C. Trace Amounts of Co_3O_4 Nano-Particles Modified TiO_2 Nanorod Arrays for Boosted Photoelectrocatalytic Removal of Organic Pollutants in Water. *Nanomaterials* **2021**, *11*, 214. https://doi.org/10.3390/nano11010214

Received: 30 November 2020
Accepted: 4 January 2021
Published: 15 January 2021

1. Introduction

From the comprehensive point of view, semiconductor metal oxides have been widely used as stable photo-catalysts for the cosmopolitan energy crisis [1–5]. TiO_2 is the most extensively used semiconductor photo-catalyst owing to its exceptional properties, such as high photo-catalytic activity, chemical stability, environmental-friendliness, and low cost [3,4,6–8]. However, because of the large bandgap of TiO_2 (3.2 eV), the practical applications are hampered by its low electrical conductivity, strong reflection, and weak light-harvesting ability [9,10], as well as the rapid combination of photo-generated electron and hole pairs. Various strategies have been utilized to improve the photo-catalytic efficiency of TiO_2 materials, such as tuning their crystallite size and structure, sensitizing them by organic dye and quantum dots [8,11,12], and modifying them with metals (e.g., Pt, Ru, Ag, Au, Rh, Pd, Ni, and Co) [3,10,13–17] or transition metal oxides (e.g., Co_3O_4, CoO, Cu_2O, and Fe_2O_3) [18–21] with a narrow band gap semiconductor. The formation of hetero-junctions between metal oxides and semiconductors is a useful strategy to suppress the recombination of photo-generated electrons and holes in TiO_2, and extend photon absorption into the visible regime, which can enhance the photochemical efficiency of TiO_2 nanomaterials.

Semiconductor-based hetero-junctions are able to facilitate fast charge separation and enhance the photo-catalytic efficiency of TiO_2 nanomaterials. It is an effective strategy to construct TiO_2-based hetero-junction structures with transition metal oxides. Heterojunction structures have the potential to facilitate electron–hole separation. TiO_2 is a n-type

semiconductor and, combined with a p-type semiconductor in a suitable band gap position to form a p-n heterojunction, it is an effective tactic to expand light absorption, enhance the separation effects of electrons and holes, prolong the lifetime of the electron and hole, and heighten the photocatalytic activity. Transition metal oxides, such as Ag_2O, Cu_2O, CuO, and Co_3O_4, have been used to form a p-n junction to promote an interfacial electron transfer process and increase the separation effect [18,22–24]. Cobalt oxides have received attention because of their excellent photo-catalytic activity in carbon dioxide reduction, oxygen reduction, and environment restoration [25,26]. Based on its properties of outstanding photocatalytic activity and low cost, cobalt oxide becomes a feasible material to fabricate the heterojunction structure with other semiconductor photocatalysts. In this work, the Co_3O_4-TiO_2 nanorod arrays were synthesized by photochemical deposition (a green method). The performance of Co_3O_4-TiO_2 nanorod arrays could be controlled by adjusting the pH value and the concentration of the Co precursor.

2. Experimental

2.1. Preparation of TiO_2 Nanorod Arrays

The TiO_2 nanorod arrays on Fluorine doped tin oxide (FTO) were fabricated through the modified hydrothermal method [7,8]. Typically, 30 mL HCl (6 mol/L) was mixed with 0.4 mL tertrabutyl titanium by strong stirring for 10 min. Then, the above solution was transferred into a Teflon pot, in which an FTO glass electrode with the coated layer facing down was placed against the wall of the Teflon pot. The hydrothermal synthesis was carried out at 150 °C for 6 h in an oven. Then, the TiO_2 nanorod arrays was washed with high pure water, and dried by high pure N_2.

2.2. Fabrication of Ultra Small Co_3O_4 Coated TiO_2 Nanorod Arrays

The Co_3O_4-coated TiO_2 nanorod arrays were prepared by photo-chemical deposition in a 1:1 ethanol/water solution containing different concentrations of $Co(NO_3)_2$ under Xe lamp with a powder intensity of 100 mW/cm^2. The driving force of the Co deposition on the TiO_2 nanorod arrays was high energetic photons, which could photo-excite electrons from the valance band of TiO_2 to the conductor band and leave holes on the valance band. The holes were depleted by the hole receptor of ethanol. The electrons can reduce the cobalt ions onto the surface of TiO_2 nanorod arrays. Nano cobalt metal was stable and easily oxidized to Co_3O_4.

2.3. Photo-Electrochemical Studies of the Co_3O_4 Modified TiO_2 Nanorod Arrays

To study the photo-electrochemical response of the Co_3O_4-modified TiO_2 nanorods and pure TiO_2 nanorod arrays (1.0 cm × 1.0 cm), open circuit potential (OCP) and the ampere-metric method (*I*–*T*) were conducted in 0.1 mol/L Na_2SO_4 solution at room temperature after being deoxidized by high pure N_2 for 15 min.

2.4. The Photo-Electrochemical Degradation Research

Methylene blue and hydroquinone were used to test the photo-electrochemical activity of Co_3O_4 modified TiO_2 nanorod arrays and pure TiO_2 nanorod arrays. The Co_3O_4 modified TiO_2 and pure TiO_2 nanorod arrays with a geometric area of 1.0 cm × 1.0 cm were used as the working electrode, as well as platinum as the counter electrode and saturated calomel electrode (SCE) as the reference electrode. A 500 W Xe lamp was used to simulate sunlight with a powder intensity of 100 mW/cm^2. A solution containing 10 mg/L methylene blue or hydroquinone, 0.1 mol/L Na_2SO_4, and 10 mmol/L H_2O_2 was used as the investigated subject. During the photo-electrochemical degradation process, the electrode was added with 1.0 V bias potential (*vs*. SCE) and was light-illuminated to degrade methylene blue or hydroquinone. To avoid the effects of solution temperature, the reaction system was placed in a constant temperature system with a circulating water device (Beijing LabTech Instruments Co., Ltd., Beijing, China). The photo-electrochemical degradation process of methylene blue and hydroquinone was measured by UV/vis spectrum.

3. Results and Discussions

3.1. XRD Analysis

The Co_3O_4-TiO_2 and TiO_2 nanorod arrays were investigated by X-ray diffraction measurement (XRD) using copper target to identify the phase of all samples. The Co_3O_4-TiO_2 and TiO_2 samples in Figure 1 show the rutile phase of TiO_2 (JCPDS No1-1292). No new XRD peaks of Co_3O_4 were observed for the Co_3O_4-TiO_2 nanorod arrays, which might because of the small amount of cobalt oxide in the Co_3O_4-TiO_2 hybrid catalyst.

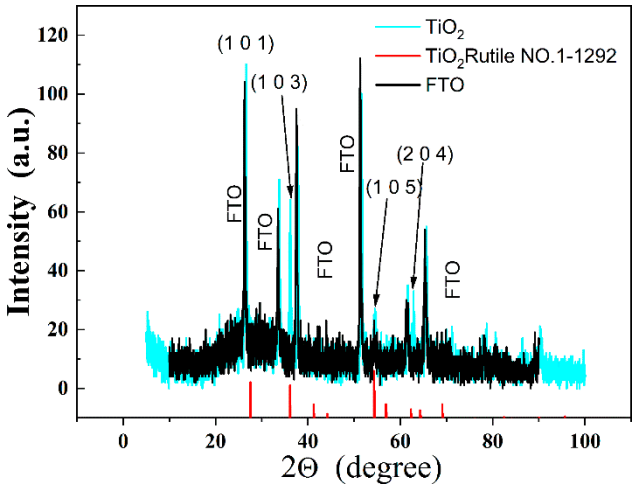

Figure 1. XRD pattern of Co_3O_4-TiO_2 nanorod arrays and pure TiO_2 nanorod arrays.

3.2. Scanning Electron Microscopy (SEM) and Transmission Electron Microscopy (TEM) Measurement

The morphologies and microstructures of the TiO_2 nanorod arrays and Co_3O_4-TiO_2 nanorod arrays were characterized by scanning electron microscopy (SEM). Figure 2 shows the top view SEM images of the TiO_2 and Co_3O_4-TiO_2 nanorod arrays. Highly ordered and large scale TiO_2 nanorod arrays are vertically aligned on both pure TiO_2 and Co_3O_4-TiO_2 nanorod arrays in Figure 2.

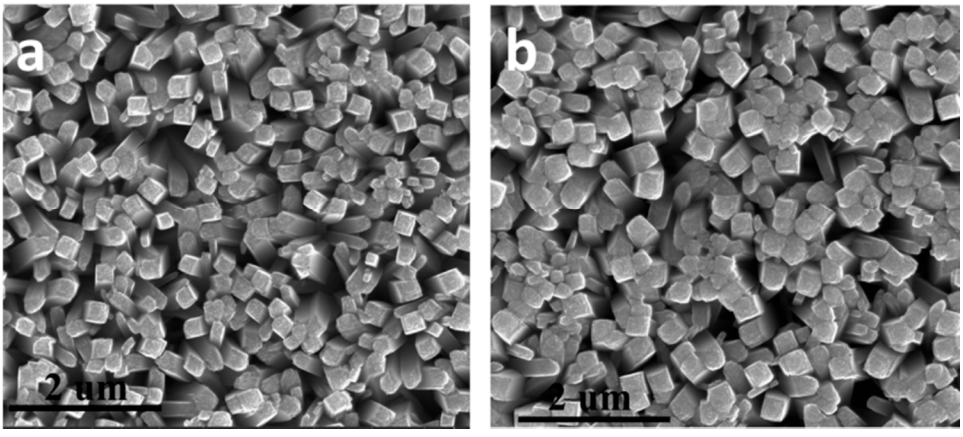

Figure 2. Scanning electron microscopy (SEM) images of (**a**) TiO_2 nanorod arrays and (**b**) Co_3O_4-TiO_2 nanorod arrays.

The average diameter of TiO_2 nanorod is about 180 nm with a rectangular cross section. There are almost no different features between Co_3O_4-TiO_2 nanorod arrays and pure TiO_2 nanorod arrays, which might because of the small amount of Co element in the Co_3O_4-TiO_2 nanorod arrays. The small amount of Co element could be confirmed by Energy Dispersive X-ray (EDX) in Supplementary Materials Figure S1. Compared with the super strong signal

of Ti and O element, the signal of Co element was very low, which means the cobalt content was very low.

Figure 3a–d show the TEM images of TiO_2 nanorods and Co_3O_4-TiO_2 nanorod arrays, respectively. It can be clearly seen that the TiO_2 nanorod arrays have the dimension of 4 nm with a clearly lattice structure. Figure 3b is the high resolution of TEM image of TiO_2. Compared with the clear lattice structure of pure TiO_2 nanorods, the surface of Co_3O_4-TiO_2 nanorod arrays (Figure 3c) was covered with something similar to fog, which makes the lattice structure of Co_3O_4-TiO_2 nanorods not obvious. High resolution TEM of Co_3O_4-TiO_2 nanorod in Figure 3d showed that there were some amorphous Co_3O_4 on the surface of TiO_2.

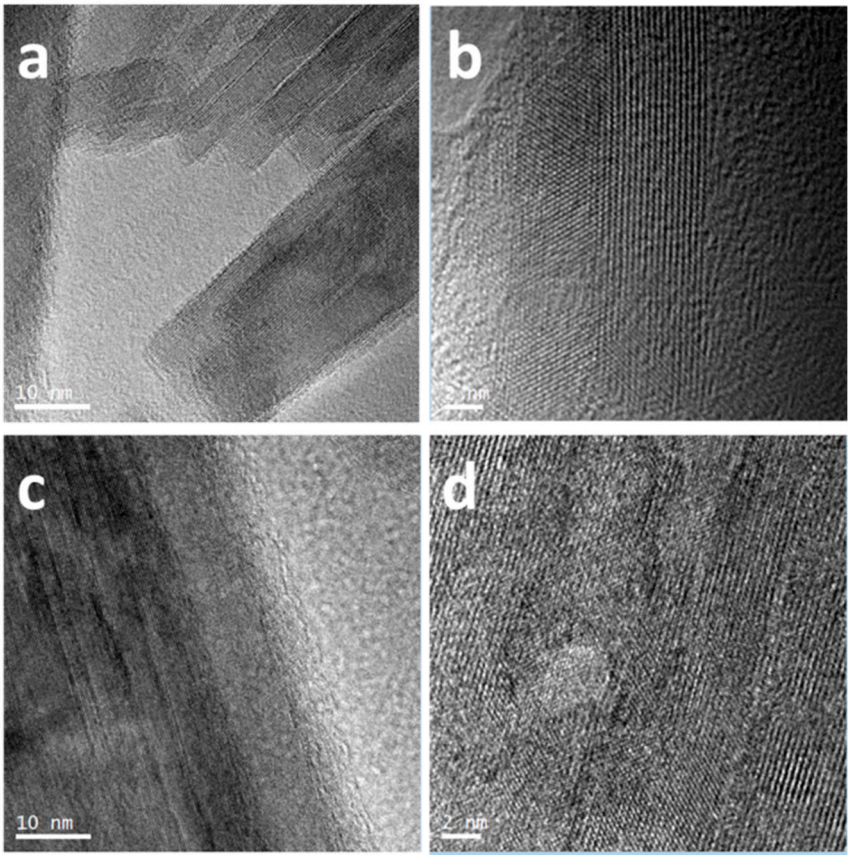

Figure 3. TEM and high resolution TEM of TiO_2 nanorod arrays (**a**,**b**) and Co_3O_4-TiO_2 nanorod arrays (**c**,**d**).

3.3. X-ray Photoelectron Spectroscopy (XPS) Analysis

To confirm the composition of Co_3O_4-TiO_2 nanorod arrays sample, the XPS method was used to study the chemical composition and valence state of Co_3O_4-TiO_2. The survey spectra illustrated in Supplementary Materials Figure S2 demonstrates the existence of Co, Ti, and O elements. Figure 4a shows the XPS spectrum of O $_{1s}$. Figure 4b shows the XPS spectrum of Ti 2p obital of the Co_3O_4-TiO_2 nanorod array. The Ti $2p_{3/2}$ and $2p_{1/2}$ located at 458.4 eV and 464.1 eV can be assigned to Ti^{4+}, which coincided with TiO_2. The band energy of 780.50 eV and 797.43 eV in Figure 4c corresponded to Co $2p_{3/2}$ and Co $2p_{1/2}$, respectively. The peaks are the typical signature of Co_3O_4 and are consistent with the previous literature [27]. Compared with the strong intensity of the Ti and O element, the XPS spectra strength of cobalt was very weak, which meant the amount of cobalt element in Co_3O_4-TiO_2 nano-materials was small.

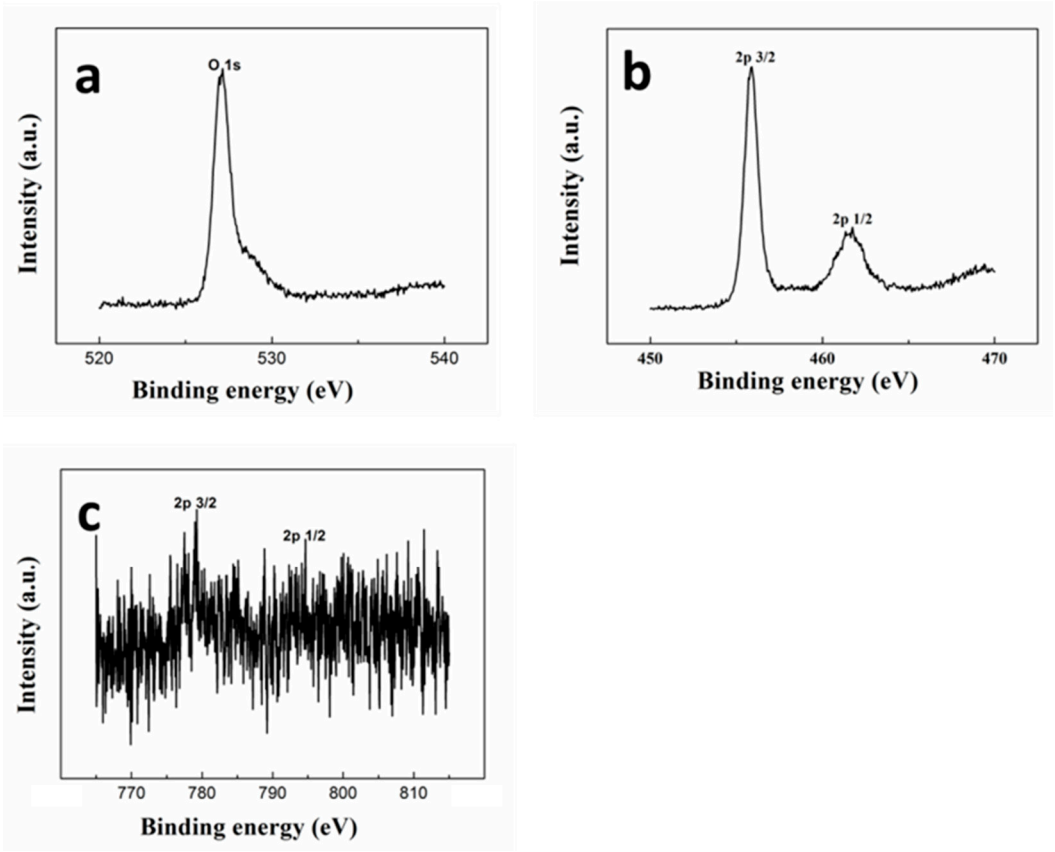

Figure 4. The XPS spectra of Co_3O_4-TiO_2 nanorod arrays: (**a**) O $_{1s}$, (**b**) Ti_{3d}, and (**c**) Co_{2p}.

The experimental data were in accordance with the EDX results in Supplementary Materials Table S1. The amount of Co was small, because of the high activity of cobalt metal. Cobalt element is more vivacious than hydrogen element, which means there is a competitive reaction between cobalt ions and hydrogen ions during photochemical deposition. The competition between cobalt ions and hydrogen ions decreases the amount of cobalt deposition on the TiO_2 surface. Furthermore, the Co metal easily dissolved into Co ions under acid circumstance. Therefore, the competitive reaction and the instability of cobalt lead to the ultra-small amount of Co on the TiO_2 nanorod arrays.

3.4. Photocurrent Test

The transient photocurrent was further used to confirm the generation, transfer, and separation processes of the photo-induced electrons and holes on both Co_3O_4 modified TiO_2 nanorod arrays and the pure TiO_2 nanorod arrays. To illustrate the effect of Co_3O_4 on photocatalytic activity of Co_3O_4-TiO_2 nanorod array, the photocurrent response of the TiO_2 nanorod arrays and Co_3O_4-TiO_2 nanorod arrays was measured by chopping light. The curves of both Co_3O_4-TiO_2 and TiO_2 samples in Figure 5a had outstanding responses to chopping light cycles. The current value of Co_3O_4-TiO_2 is five times higher than pure TiO_2 nanorod arrays. This means that the Co_3O_4-TiO_2 nanorod arrays had higher photoelectrocatalytic activity than the pure TiO2 nanorod arrays.

Compared with pure TiO_2 nanorod arrays, the Co_3O_4-TiO_2 nanorod arrays exhibited an obviously higher photocurrent, which indicated that Co_3O_4-TiO_2 nanorod arrays had the higher photo-electrochemical activity. Under light illumination, the electron in the valence band was excited to the conductor band and left a hole in the valence band. The electrons were accumulated on the conductor band and holes were assembled on the valence band by persistent light illumination [28]. The relative OCP value of the samples was measured to compare the performance in a different semiconductor. In comparison, the relative OCP value of Co_3O_4-TiO_2 was higher than the pure TiO_2 nanorod arrays, which

demonstrated that separation of e-h$^+$ pairs in the Co_3O_4-TiO_2 heterojunction is significantly improved by the addition of Co_3O_4 (Supplementary Materials Figure S3).

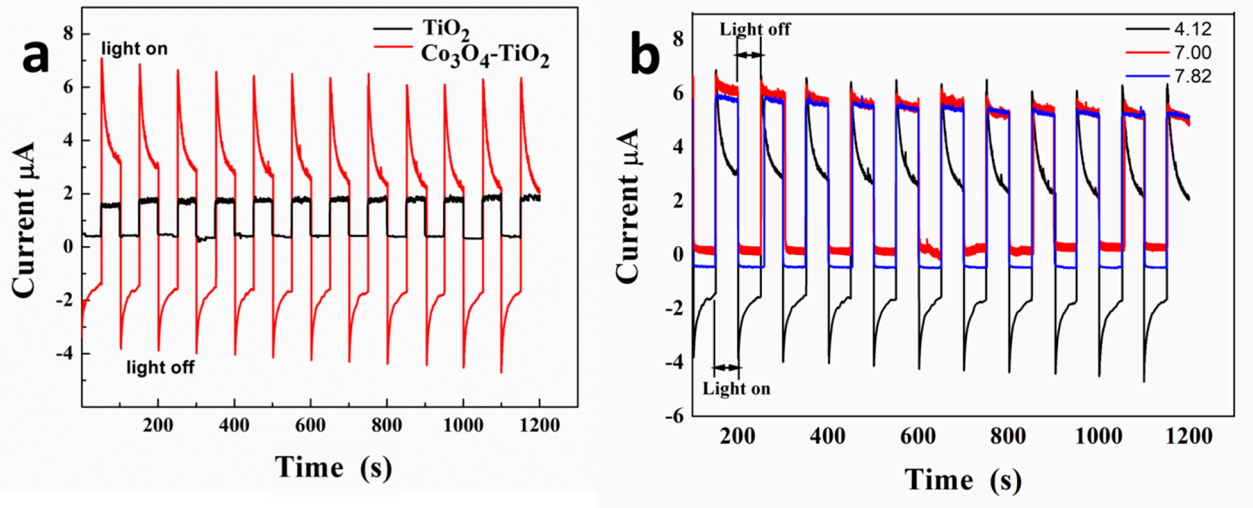

Figure 5. The *I*–*T* curves measured at applied potential of 0 V *vs.* saturated calomel electrode (SCE) under chopped illumination in 0.1 mol/L Na_2SO_4 solution: (**a**) TiO_2 and Co_3O_4-TiO_2 fabricated at pH 4.12; (**b**) Co_3O_4-TiO_2 fabricated at different pH value.

3.5. The Formation Mechanisms of Co_3O_4 Nanoparticles

Further observation found that Co_3O_4-TiO_2 nanorods fabricated in different pH values had diverse responses to visible light, as shown in Figure 5b. The Co_3O_4-TiO_2 nanorods fabricated under pH 4.12 had the highest photo-electrochemical response compared with others fabricated at pH 7.82 and 7.00. The formation mechanisms of Co_3O_4 nanoparticles in different pH solutions were different, which led to a different response to visible light. In neutral solution, the Co_3O_4 were formed under photochemical deposition.

$$3Co - 8e^- + 4H_2O = Co_3O_4 + 8H^+ \quad (1)$$

Co nanoparticles were easily deposited onto the semiconductor in alkaline solution. Such as Co-ZnO was fabricated, which had high catalytic activity in oxygen production [29]. And the high catalytic activity of Ni-CdS nanorods was fabricated through photochemical deposition in NaOH solution containing Ni ions and methanol [30]. Holes have high energy, which could oxidize methanol adsorbing on the semiconductor. Considering the high concentration of ethanol, ethanol was oxidized to formaldhyde and holes were decomposed. It is very difficult to deposit transition metal or metal oxide onto semiconductors in the acid solution because cobalt metal is more active than the hydron element. There were two different competitive reactions during the photodeposition reaction. They are listed below:

$$Co^{2+} + 2e^- = Co \quad (2)$$

$$2H^+ + 2e^- = H_2 \quad (3)$$

Furthermore, the high activity of transition metals meant they easily dissolved in acid solution. The Co metal was not stable because of oxidization reaction and photocorrosion. Considering the above reasons, the amount of Co is very small.

$$Co - 2e^- = Co^{2+} \quad (4)$$

$$3Co - 8e^- + 4OH^- = Co_3O_4 + 4H^+ \quad (5)$$

In alkaline solution, the Co ions mainly existed through $Co(OH)_4^{2-}$, which was reduced to Co metal by electrons photo-excited on the TiO_2 surface. The Co metal was not stable and could easily be oxidized to Co_3O_4 by oxygen or OH radical produced in photochemical deposition.

$$Co(OH)_4^{2-} + 2e^- = Co + 4OH^- \quad (6)$$

The amount of Co_3O_4 can be controlled through regulating the concentration of Co ions from 0.1 mmol/L to 1 mmol/L. We found that Co_3O_4-TiO_2 nanorod array fabricated in 0.5 mmol/L cobalt ions had the highest photocatalytic activity. It can be clearly seen that the photocurrent increased with the concentration of Co ions increasing from 0.1 mmol/L to 0.5 mmol/L (in Figure 6). However, the photo-electrochemical currents decreased when the Co ions' concentrations were further increased, which may be because of the formation of a thick Co_3O_4 layer and increase in the carrier recombination rate.

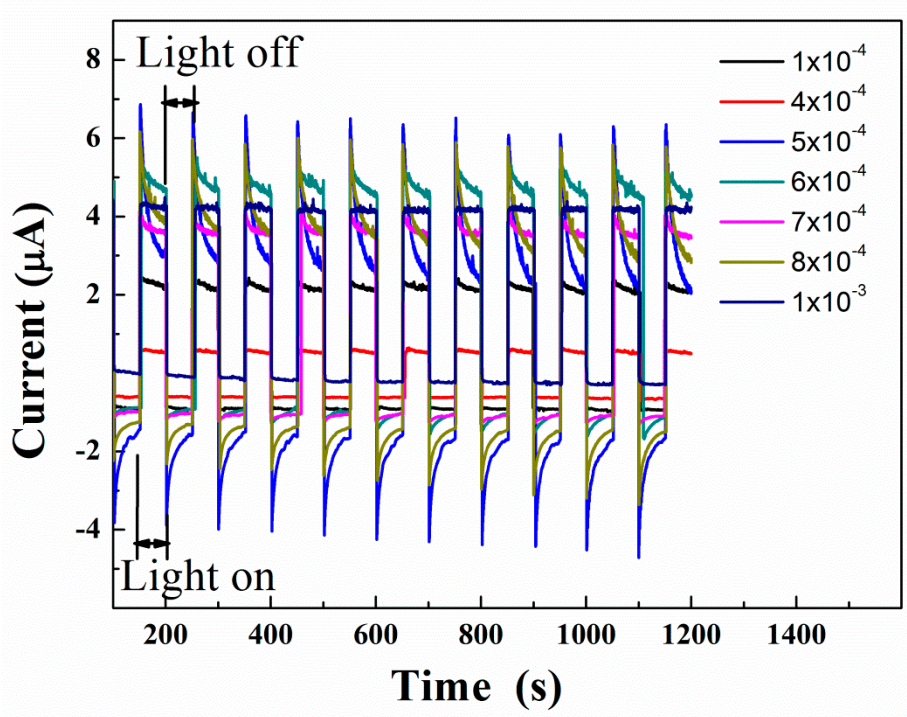

Figure 6. Open circuit potential (OCP) curve of Co_3O-TiO_2 fabricated in different concentrations of Co ions.

3.6. Photo-Electrochemical Activity of Co_3O_4 Modified TiO_2 Nanorod Arrays

Methylene blue was used as the probe to evaluate the photo-electrochemical activity of pure TiO_2 nanorod arrays and Co_3O_4 modified TiO_2 nanorod arrays. As shown in Figure 7, the TiO_2 nanorod array exhibits a moderate catalytic performance for the photo-electrochemical degradation of methylene blue, which could have contributed to the ordered arrays effect. The Co_3O_4 modified TiO_2 nanorod arrays exhibit excellent photo-electrochemical degradation activity to methylene blue. TiO_2 nanorod arrays modified with Co_3O_4 had good photochemical catalytic activity, which was attributed to the disjunction of Co_3O_4-TiO_2 and the charge transfer between Co_3O_4 and TiO_2 nanometer rod components. Furthermore, the isolated Co_3O_4 islands on the surface of TiO_2 nanorod arrays acted as reactive sites to enhance the photo-electrochemical activity. The degradation of methylene blue by Co_3O_4 modified TiO_2 was greater than that of pure TiO_2 nanorod arrays. Methylene blue was totally degraded on Co_3O_4 modified TiO_2 nanorod arrays. Compared with Co_3O_4-TiO_2 nanorod arrays, only 60% methylene blue was degraded on pure TiO_2 nanorod arrays.

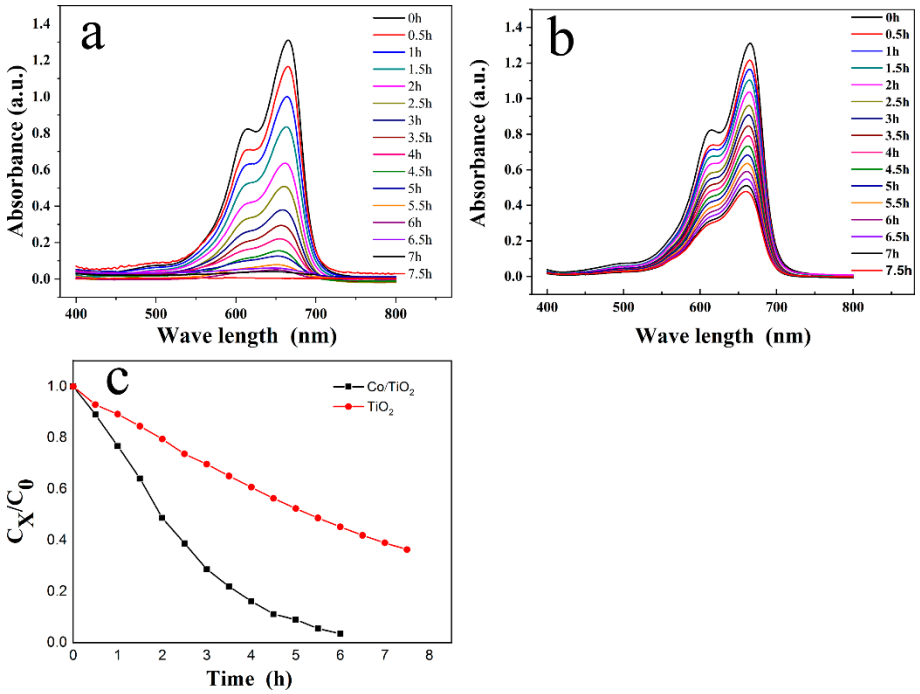

Figure 7. Photo-electrochemical degradation of methylene blue on Co_3O_4-TiO_2 and TiO_2 nanorod arrays: (**a**) Co_3O_4-TiO_2; (**b**) TiO_2 nanorod arrays; and (**c**) full curve of methylene blue degradation on Co_3O_4-TiO_2 and pure TiO_2.

The TiO_2 nanorod arrays only absorbed ultraviolet photons to generate e-h^+ pairs to degrade the methylene blue molecule, while Co_3O_4-TiO_2 nanorod arrays provide a p-n junction between Co_3O_4 nanoparticles and TiO_2 nanorod arrays. The enhancement of photo-electrochemical activity of Co_3O_4/TiO_2 heterojunction samples could have contributed to the formation of the type-II p-n hetero-junction between Co_3O_4 and TiO_2. TiO_2 is an n-type wide band gap semiconductor with the conduction band at 0.14 V, and Co_3O_4 is a p-type narrow band gap with band energy of 2.07 eV [31]. When Co_3O_4 nanoparticles are deposited onto the surface of TiO_2 nanorod arrays, a p-n heterojunction can be formed at the surface of TiO_2 nanorod arrays, and the electrons can be transferred from the Co_3O_4 to TiO_2 nanorod arrays until their Fermi levels are equal [32]. The equilibrium can be broken by methylene blue, which acted as a holes receptor. With the photo-electrochemical reaction going on, methylene blue was degraded. The positive potential was loaded onto the Co_3O_4-TiO_2 electrode to further increase the efficiency of the separation of hole and electrons. The Co_3O_4 has Co^{2+} and Co^{3+} valence state. Co^{2+} and Co^{3+} can be easily oxidized to Co^{4+}, and Co^{4+}/Co^{3+} had high activity to oxidize methylene blue to water and carbon dioxide. Thus, Co_3O_4-TiO_2 had higher photo-electrochemical activity than pure TiO_2 nanorod arrays.

Hydroquinone was used to further study the photo-electrochemical activity of Co_3O_4 modified TiO_2 and pure TiO_2 nanorod arrays. It can be seen clearly from Figure 8a,b that, compared with pure TiO_2, the Co_3O_4 modified TiO_2 nanorod arrays had higher photo-electrochemical activity. Only 30% hydroquinone was degraded on pure TiO_2 nanorod arrays, and hydroquinone displayed total degradation on Co_3O_4 modified TiO_2 nanorod arrays.

In order to clearly measure the photo-electrochemical activity of Co_3O_4 modified TiO_2 nanorod arrays and pure TiO_2 nanorod arrays, the corresponding kinetic constant was computed through fitting the experimental degradation of hydroquinone by the following equation.

$$-\ln\left(\frac{C_t}{C_0}\right) = kt \quad (7)$$

where C_t is the concentration of hydroquinone at a certain reaction time, C_0 is the original concentration, k is the apparent first rate, and t is photo-electrochemical time. The model was suitable for the photo-electrochemical hydroquinone degradation process. The k-values for the Co_3O_4-TiO_2 and pure TiO_2 nanorod arrays are 0.91745 and 0.1206, respectively. The k-value of Co_3O_4-TiO_2 is almost eight times that of the pure TiO_2 nanorod arrays, which further confirmed that Co_3O_4 addition greatly enhanced the photo-electrochemical activity.

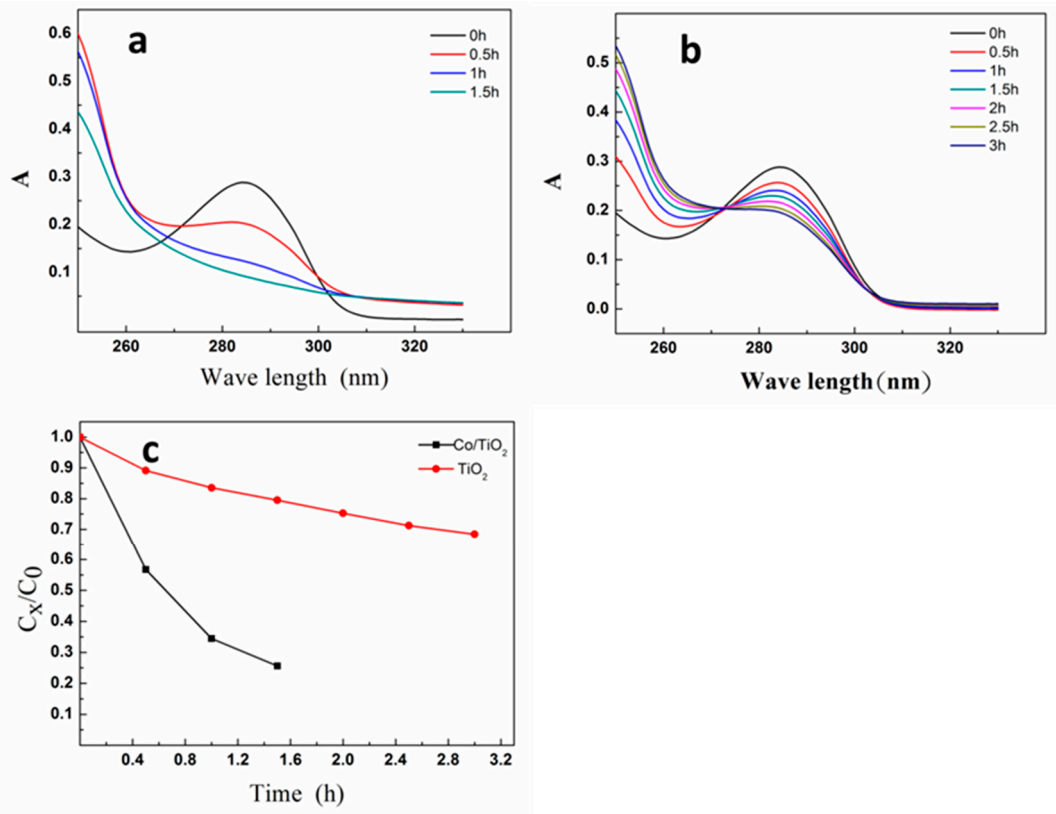

Figure 8. (**a**) Hydroquinone degradation on Co_3O_4-TiO_2 nanorod arrays; (**b**) hydroquinone degradation on pure TiO_2 nanorod arrays; and (**c**) comparison of degradation rate of hydroquinone on Co_3O_4-TiO_2 nanorod arrays and pure TiO_2 nanorod arrays.

3.7. Photo-Electro-Catalytic Degradation Mechanism

The photo-electrochemical activity of the photo-catalyst was mainly determined by light absorption, charges holes separation, and charge transfer from the inner to the surface of catalyzer. The band gap of the semiconductor was the key factor, which had a great influence on the photo-activity of the catalyst. The bandgap of Co_3O_4-TiO_2 nanorod arrays and pure TiO_2 nanorod arrays was determined from UV/vis diffuse reflectance spectra using the Tauc function, as shown in Figure 9a. The bandgap of TiO_2 nanorod arrays is 3.2 eV and is very close to that from the former literature [33]. The bandgap of Co_3O_4-TiO_2 is 2.85 eV, which could have contributed to the intrinsic narrow band gap of Co_3O_4 hybrid with TiO_2. The addition of Co_3O_4 reduced the band gap of the nanomaterial and then enhanced its catalytic activity.

The influence of Co_3O_4 on the energy level of the photo-catalyst was studied through the Mott–Schottky electrochemical method in 0.1 mol/L Na_2SO_4 with 1000 Hz for Co_3O_4-TiO_2 and pure TiO_2 nanorod arrays. Both TiO_2 and Co_3O_4-TiO_2 had positive slopes, meaning that both pure TiO_2 and Co_3O_4-TiO_2 are n-type semiconductors and electrons as the majority carriers. It can be seen that the addition of Co_3O_4 did not change the semiconductor type of TiO_2, but greatly changed the Fermi level and the flat band potential of TiO_2. This phenomenon is consistent with other reported work that the addition of cobalt

would change the band energy of the nanomaterial [34]. The flat-band potential (V_b) and the carrier density of nano-materials can be calculated according to the following equation:

$$N_D = \frac{2}{e\varepsilon 0\varepsilon}\left(\frac{dE}{d\left(\frac{1}{C^2}\right)}\right) \quad (8)$$

where e_0 is the dielectronic constant of the material, ε is the permittivity of the vacuum, e is the element charge, N_D is the donor density, and C is the capacitance. From the slope in the plot of $1/C^2$ versus V in the Figure 9b, the smaller slope for the Co_3O_4-TiO_2 reflects a higher electron donor density. The higher N_D means lower resistance, faster charge transfer, and higher electrochemical activity.

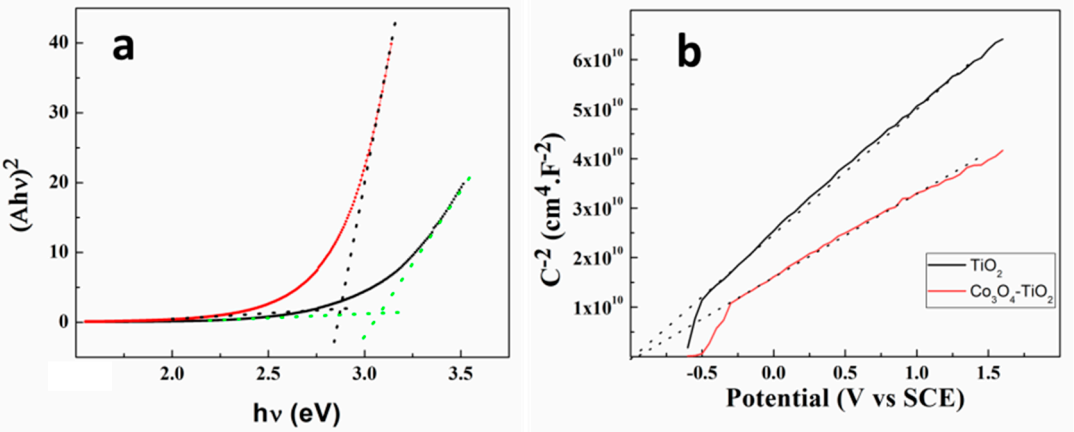

Figure 9. (**a**) Plots of $(ahv)^2$ *vs.* photo energy of Co_3O_4-TiO_2 and TiO_2 nanorod arrays. (**b**) Mott–Schottky plots of Co_3O_4-TiO_2 and pure TiO_2 nanorod arrays in 0.5 mol/L Na_2SO_4 at a frequency of 1 KHz.

The Co_3O_4-TiO_2 nanorod arrays had greatly enhanced photo-electrochemical performance, which could be attributed to the synergetic effects of the formation of a p-n junction between Co_3O_4 and TiO_2. The catalytic performance of semiconductor nanomaterials depends on the bandgap of the semiconductor nanomaterial, the separation of electrons and holes, and the lifetime of electrons and holes generated by photo exciting. The hole and electron can move the surface to react with the adsorbed reactant. However, the electron and hole could recombine easily in a short time, which greatly abates the activity of the catalyst. Therefore, the catalyst's activity can be greatly influenced by the life-time of the photo-induced electron-holes pairs. The p-n junction could greatly enhance the life-time of the electron and holes. The longer life-time of holes and electrons greatly enhances the activity of catalysts. Co_3O_4 is a p-type semiconductor with a band gap of 2.19 eV [31], while TiO_2 is an n-type semiconductor with a band gap of 3.2 eV [1]. Thus, Co_3O_4 participating in the TiO_2 nanorod arrays could change the structure of TiO_2 in three aspects: (1) broaden the absorption range from ultraviolet light to visible light; (2) form a p-n junction to enhance the life-time of the electron; or (3) the disjunct Co_3O_4 nanoparticles act as an activation point to improve the photo-electrochemical activity. The conduction band (CB) position of TiO_2 is more anodic than Co_3O_4, so the excited electrons on the CB of TiO_2 could not transfer to Co_3O_4, while the holes could transfer from TiO_2 to Co_3O_4. The recombination of electron and hole could be reduced just as shown in Scheme 1. At the hetero-junction in thermal equilibrium, the p-type and n-type regions have completely opposite charges, and the n-type regions become positive, while the p-type region becomes negative. When the n-p hetero-junction semiconductor is excited by visible light with high energy to band gap, the photo-generated electrons can move to the CB of the n-type TiO_2 and holes can move to the VB of the n-type semiconductor for the formation of the inner electric field in the Co_3O_4/TiO_2 sample, which effectively impedes the recombination of electron–hole pairs. The biased voltage could further restrain the photo-excited electrons and holes

recombination through the following mechanism. The positive bias voltage depletes the electrons and, as a result, the holes can be excluded to the surface. Then, the absorbed molecules on the surface of Co_3O_4 can react with the holes to form a series of radicals, such as OH radical and other radicals. These radicals have great energy to oxidize the organic waste to water and carbon dioxide.

$$Co_3O_4 + \text{visible light} \rightarrow Co_3O_4(e^-) + Co_3O_4(h^+) \quad (9)$$

$$TiO_2 + \text{bias voltage} \rightarrow TiO_2(h^+) \quad (10)$$

$$Co_3O_4 + \text{bias voltage} \rightarrow Co_3O_4 + \text{holes} \quad (11)$$

$$H_2O_2 + \text{hole} \rightarrow 2OH \quad (12)$$

$$MB + 2OH \rightarrow CO_2 + H_2O \quad (13)$$

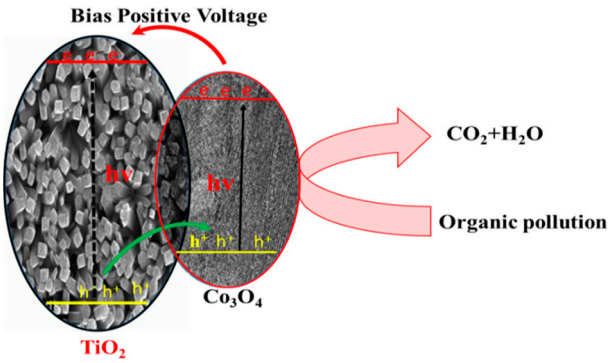

Scheme 1. Schematic mechanism of the photo-electrochemical degradation of organic pollution on Co_3O_4-TiO_2 at a constant positive bias potential.

According to the above results and discussion, consequently, under external bias voltage, electrons transfer along the external wires to auxiliary electrode and leave holes on the surface of Co_3O_4, which could oxidize the organic waste to water and carbon dioxide, as the schematic shows.

4. Conclusions

Ultra small amounts of Co_3O_4-modified TiO_2 nanorod arrays were successfully fabricated thorough green photochemical deposition methods without adding any nocuous reagents. The Co_3O_4/TiO_2 nanorod arrays fabricated in acid solution had the highest photo-electrochemical activity. We elaborated on the mechanism of Co_3O_4-TiO_2 fabricated in different pH value solutions. The amount of Co_3O_4 could be controlled by adjusting the concentration of Co ions. The small amount of Co_3O_4 made many disjunct active points, which acted as active sites to mineralize organic wastes during photoelectrochemical degradation. The Co_3O_4/TiO_2 nanorod arrays had higher photo-electrochemical activity to degrade organic waste than pure TiO_2 nanorod arrays, which had great potential in waste water treatment.

Supplementary Materials: The following are available online at https://www.mdpi.com/2079-4991/11/1/214/s1, Figure S1: EDX of Co_3O_4 modified TiO_2 nanorod arrays, Figure S2: Full XPS data of Co_3O_4 modified TiO_2 nanorod arrays, Figure S3: OCP response of Co_3O_4 modified TiO_2 nanorod arrays fabricated in different pH value. Table S1: the content of Co_3O_4 modified TiO_2 nanorod arrays.

Author Contributions: Conceptualization, Z.Z. and C.W.; methodology, Y.D.; software, X.Z.; validation, Z.Z., Y.D. and C.W.; formal analysis, Y.D.; in-vestigation, W.C.; resources, Y.D.; data curation, C.L.; writing—original draft preparation, Y.D.; writing—review and editing, Z.Z.; visualization, C.L.; supervision, Z.Z.; project administration, Z.B.; funding acquisition, Z.Z. All authors have read and agreed to the published version of the manuscript.

Funding: This research was funded by National Natural Science Foundation of China (51862029), Lanzhou Talent Innovation and Entrepreneurship Project (2019-RC-99), Industry Support and Guidance Project for Colleges and Universities in Gansu Province in 2020 (2020C-32), and Major Scientific Projects of Gan Su Institute of Political Science and Law (GZF2018XZD03).

Informed Consent Statement: Informed consent was obtained from all subjects involved in the study.

Data Availability Statement: Data is contained within the article or Supplementary Material.

Conflicts of Interest: The authors declare no conflict of interest.

References

1. Naldoni, A.; Allieta, M.; Santangelo, S.; Marelli, M.; Fabbri, F.; Cappelli, S.; Bianchi, C.L.; Psaro, R.; Dal, V.S. Effect of nature and location of defects on bandgap narrowing in black TiO_2 nanoparticles. *J. Am. Chem. Soc.* **2012**, *134*, 7600–7603. [CrossRef]
2. Khan, S.U.; Shahry, M.; Ingler, W.B., Jr. Efficient photochemical water splitting by a chemically modified n-TiO_2. *Science* **2002**, *297*, 2243–2245. [CrossRef] [PubMed]
3. Neatu, S.; Macia, A.J.A.; Concepcion, P.; Garcia, H. Gold-copper nanoalloys supported on TiO_2 as photocatalysts for CO_2 reduction by water. *J. Am. Chem. Soc.* **2014**, *136*, 15969–15976. [CrossRef] [PubMed]
4. Yang, L.; Luo, S.; Li, Y.; Xiao, Y.; Kang, Q.; Cai, Q. High efficient photocatalytic degradation of p-nitrophenol on a unique Cu_2O/TiO_2 p-n heterojunction network catalyst. *Environ. Sci. Technol.* **2010**, *44*, 7641–7646. [CrossRef] [PubMed]
5. Lu, W.; Zhang, Y.; Zhang, J.; Xu, P. Reduction of Gas CO_2 to CO with High Selectivity by Ag Nanocube-Based Membrane Cathodes in a Photoelectrochemical System. *Ind. Eng. Chem. Res.* **2020**, *59*, 5536–5545. [CrossRef]
6. Dhandole, L.K.; Mahadik, M.A.; Kim, S.G.; Chung, H.S.; Seo, Y.S.; Cho, M.; Ryu, J.H.; Jang, J.S. Boosting Photocatalytic Performance of Inactive Rutile TiO_2 Nanorods under Solar Light Irradiation: Synergistic Effect of Acid Treatment and Metal Oxide Co-catalysts. *ACS Appl. Mater. Interfaces* **2017**, *9*, 23602–23613. [CrossRef]
7. Huang, H.; Pan, L.; Lim, C.K.; Gong, H.; Guo, J.; Tse, M.S.; Tan, O.K. Hydrothermal Growth of TiO_2 Nanorod Arrays and In Situ Conversion to Nanotube Arrays for Highly Efficient Quantum Dot-Sensitized Solar Cells. *Small* **2013**, *9*, 3153–3160. [CrossRef]
8. Li, J.; Cushing, S.K.; Zheng, P.; Senty, T.; Meng, F.; Bristow, A.D.; Manivannan, A.; Wu, N. Solar hydrogen generation by a CdS-Au-TiO_2 sandwich nanorod array enhanced with Au nanoparticle as electron relay and plasmonic photosensitizer. *J. Am. Chem. Soc.* **2014**, *136*, 8438–8449. [CrossRef]
9. Liu, J.; Li, Y.; Ke, J.; Wang, S.; Wang, L.; Xiao, H. Black NiO-TiO_2 nanorods for solar photocatalysis: Recognition of electronic structure and reaction mechanism. *Appl. Catal. B Environ.* **2018**, *224*, 705–714. [CrossRef]
10. Mishra, S.; Yogi, P.; Sagdeo, P.R.; Kumar, R. TiO_2–Co_3O_4 Core–Shell Nanorods: Bifunctional Role in Better Energy Storage and Electrochromism. *ACS Appl. Energy Mater.* **2018**, *1*, 790–798. [CrossRef]
11. Yang, M.; Ding, B.; Lee, S.; Lee, J.K. Carrier Transport in Dye-Sensitized Solar Cells Using Single Crystalline TiO_2 Nanorods Grown by a Microwave-Assisted Hydrothermal Reaction. *J. Phys. Chem. C* **2011**, *115*, 14534–14541. [CrossRef]
12. Li, T.L.; Lee, Y.L.; Teng, H. CuInS2 quantum dots coated with CdS as high-performance sensitizers for TiO_2 electrodes in photoelectrochemical cells. *J. Mater. Chem.* **2011**, *21*, 5089–5098. [CrossRef]
13. Zhang, J.; Jin, X.; Morales, G.P.I.; Yu, X.; Liu, H.; Zhang, H.; Razzari, L.; Claverie, J.P. Engineering the Absorption and Field Enhancement Properties of Au-TiO_2 Nanohybrids via Whispering Gallery Mode Resonances for Photocatalytic Water Splitting. *ACS Nano* **2016**, *10*, 4496–4503. [CrossRef] [PubMed]
14. Biyoghe, L.; Ndong, B.; Ibondou, M.P.; Gu, X.; Lu, S.; Qiu, Z.; Sui, Q.; Mbadinga, S.M. Enhanced Photocatalytic Activity of TiO2 Nanosheets by Doping with Cu for Chlorinated Solvent Pollutants Degradation. *Ind. Eng. Chem. Res.* **2014**, *53*, 1368–1376. [CrossRef]
15. Sun, T.; Fan, J.; Liu, E.; Liu, L.; Wang, Y.; Dai, H.; Yang, Y.; Hou, W.; Hu, X.; Jiang, Z. Fe and Ni co-doped TiO_2 nanoparticles prepared by alcohol-thermal method: Application in hydrogen evolution by water splitting under visible light irradiation. *Powder Technol.* **2012**, *228*, 210–218. [CrossRef]
16. Seh, Z.W.; Liu, S.; Low, M.; Zhang, S.Y.; Liu, Z.; Mlayah, A.; Han, M.Y. Janus Au-TiO_2 photocatalysts with strong localization of plasmonic near-fields for efficient visible-light hydrogen generation. *Adv. Mater.* **2012**, *24*, 2310–2314. [CrossRef]
17. Melvin, A.A.; Illath, K.; Das, T.; Raja, T.; Bhattacharyya, S.; Gopinath, C.S. M-Au/TiO_2 (M = Ag, Pd and Pt) nanophotocatalyst for overall solar water splitting: Role of interfaces. *Nanoscale* **2015**, *7*, 13477–13488. [CrossRef]
18. Bessekhouad, Y.; Robert, D.; Weber, J.V. Photocatalytic activity of Cu_2O/TiO_2, Bi_2O_3/TiO_2 and $ZnMn_2O_4/TiO_2$ heterojunctions. *Catal. Today* **2005**, *101*, 315–321. [CrossRef]
19. Santamaria, M.; Conigliaro, G.; Franco, F.; Quarto, F. Photoelectrochemical Evidence of Cu_2O/TiO_2 Nanotubes Hetero-Junctions formation and their Physicochemical Characterization. *Electrochim. Acta* **2014**, *144*, 315–323. [CrossRef]

20. Kupfer, B.; Majhi, K.; Keller, D.A.; Bouhadana, Y.; Rühle, S.; Barad, H.N.; Anderson, A.Y.; Zaban, A. Thin Film Co_3O_4/TiO_2 Heterojunction Solar Cells. *Adv. Energy Mater.* **2015**, *5*, 1401007. [CrossRef]
21. Liu, L.; Ji, Z.; Zou, W.; Gu, X.; Deng, Y.; Gao, F.; Tang, C.; Dong, L. In Situ Loading Transition Metal Oxide Clusters on TiO_2 Nanosheets As Co-catalysts for Exceptional High Photoactivity. *ACS Catal.* **2013**, *3*, 2052–2061. [CrossRef]
22. Sarkar, D.; Ghosh, C.K.; Mukherjee, S.; Chattopadhyay, K.K. Three dimensional Ag_2O/TiO_2 type-II (p-n) nanoheterojunctions for superior photocatalytic activity. *ACS Appl. Mater. Interfaces* **2013**, *5*, 331–337. [CrossRef] [PubMed]
23. Shao, Z.; Zhang, Y.; Yang, X.; Zhong, M. Au-Mediated Charge Transfer Process of Ternary $Cu_2O/Au/TiO_2$-NAs Nanoheterostructures for Improved Photoelectrochemical Performance. *ACS Omega* **2020**, *5*, 7503–7518. [CrossRef] [PubMed]
24. Wang, M.; Sun, L.; Lin, Z.; Cai, J.; Xie, K.; Lin, C. P–n heterojunction photoelectrodes composed of Cu_2O-loaded TiO_2 nanotube arrays with enhanced photoelectrochemical and photoelectrocatalytic activities. *Energy Environ. Sci.* **2013**, *6*, 1211–1220. [CrossRef]
25. Zhang, G.; Huang, C.; Wang, X. Dispersing molecular cobalt in graphitic carbon nitride frameworks for photocatalytic water oxidation. *Small* **2015**, *11*, 1215–1221. [CrossRef]
26. Downes, C.A.; Marinescu, S.C. Efficient Electrochemical and Photoelectrochemical H_2 Production from Water by a Cobalt Dithiolene One-Dimensional Metal-Organic Surface. *J. Am. Chem. Soc.* **2015**, *137*, 13740–13743. [CrossRef]
27. Gao, Z.; Zhang, L.; Ma, C.; Zhou, Q.; Tang, Y.; Tu, Z.; Yang, W.; Cui, L.; Li, Y. TiO_2 decorated Co_3O_4 acicular nanotube arrays and its application as a non-enzymatic glucose sensor. *Biosens. Bioelectron.* **2016**, *80*, 511–518. [CrossRef]
28. Cho, I.S.; Chen, Z.; Forman, A.J.; Kim, D.R.; Rao, P.M.; Jaramillo, T.F.; Zheng, X. Branched $TiO_{(2)}$ nanorods for photoelectrochemical hydrogen production. *Nano Lett.* **2011**, *11*, 4978–4984. [CrossRef]
29. Steinmiller, E.M.; Choi, K.S. Photochemical deposition of cobalt-based oxygen evolving catalyst on a semiconductor photoanode for solar oxygen production. *Proc. Natl. Acad. Sci. USA* **2009**, *106*, 20633–20636. [CrossRef]
30. Simon, T.; Bouchonville, N.; Berr, M.J.; Vaneski, A.; Adrovic, A.; Volbers, D.; Wyrwich, R.; Doblinger, M.; Susha, A.S.; Rogach, A.L.; et al. Redox shuttle mechanism enhances photocatalytic H_2 generation on Ni-decorated CdS nanorods. *Nat. Mater.* **2014**, *13*, 1013–1018. [CrossRef]
31. Chang, X.; Wang, T.; Zhang, P.; Zhang, J.; Li, A.; Gong, J. Enhanced Surface Reaction Kinetics and Charge Separation of p-n Heterojunction Co_3O_4/BiVO4 Photoanodes. *J. Am. Chem. Soc.* **2015**, *137*, 8356–8359. [CrossRef] [PubMed]
32. Kibria, M.G.; Zhao, S.; Chowdhury, F.A.; Wang, Q.; Nguyen, H.P.; Trudeau, M.L.; Guo, H.; Mi, Z. Tuning the surface Fermi level on p-type gallium nitride nanowires for efficient overall water splitting. *Nat. Commun.* **2014**, *5*, 1–6. [CrossRef] [PubMed]
33. Lee, J.S.; You, K.H.; Park, C.B. Highly photoactive, low bandgap TiO_2 nanoparticles wrapped by graphene. *Adv. Mater.* **2012**, *24*, 1084–1088. [CrossRef] [PubMed]
34. Sadanandam, G.; Lalitha, K.; Kumari, V.D.; Shankar, M.V.; Subrahmanyam, M. Cobalt doped TiO_2: A stable and efficient photocatalyst for continuous hydrogen production from glycerol: Water mixtures under solar light irradiation. *Int. J. Hydrogen Energy* **2013**, *38*, 9655–9664. [CrossRef]